Development of the HondaJet

Michimasa Fujino
Honda R&D Americas, Inc., Greensboro, North Carolina 27409

Keywords: *Airplane Design*

Abstract

The HondaJet is an advanced, lightweight, business jet featuring an extra large cabin, high fuel efficiency, and high cruise speed compared to existing small business jets. To achieve the high performance goals, an over-the-wing engine-mount configuration, a natural-laminar -flow wing, and a natural-laminar-flow fuselage nose were developed through extensive analyses and wind-tunnel tests. The wing is metal, having an integral, machined skin to achieve the smooth upper surface required for natural laminar flow. The fuselage is constructed entirely of composites; the stiffened panels and the sandwich panels are co-cured integrally in an autoclave to reduce weight and cost. The prototype aircraft has been designed and fabricated. Major ground tests such as structural proof tests, control-system proof test, system function tests, and ground vibration tests have been completed. The first flight was conducted on December 3, 2003, and flight testing is currently underway. The aerodynamic, aeroelastic, structural, and system designs and the ground tests performed during the development are described.

1 Introduction

The business jet is becoming a common tool for business people. Chartering business jets, however, is still expensive and the arrival of a new generation of small jets that are more affordable to operate than conventional jets is awaited. Market surveys and focus-group interviews, conducted in five major cities in the United States, show that demand for comfort, in particular, a large cabin, as well as high fuel efficiency are critical to the success of small business-jet development. The HondaJet (Fig.1) is designed to satisfy these needs. This new aircraft has great potential to revolutionize air transportation.

A unique configuration, called an over-the-wing engine-mount configuration (OTWEM), was developed to provide a larger cabin than that of conventional configurations. By mounting the engines on the wing, the carry-through structure required to mount the engines on the rear fuselage is eliminated, which allows the cabin volume to be maximized. It was a technical challenge to employ an over-the-wing engine -mount configuration for a high-speed aircraft from both aerodynamic and aeroelastic standpoints. Extensive analytical and experime-ntal studies, however, show that an over-the-wing engine-mount configuration reduces the wave drag at high speeds and achieves higher cruise efficiency when the nacelles are located at the optimum position [1].

Fig.1 HondaJet

To reduce drag and thereby achieve higher fuel efficiency, a new natural-laminar-flow (NLF) wing [2] and a natural-laminar-flow fuselage nose were developed through theoretical and experimental studies. By employing these advanced technologies, the specific range of the HondaJet is far greater than that of existing

small jets.

To achieve natural laminar flow on the wing, surface waviness as well as steps and gaps in the wing structure must be minimized. Appropriate criteria were derived from flight tests. The upper skin is a machine-milled, integral panel that maintains the contour necessary for the achievement of laminar flow. The actual wing structure was tested in the wind tunnel to confirm that laminar flow is achieved on the actual wing surface.

To reduce weight and manufacturing costs, an advanced composite structure is used for the fuselage, consisting of a combination of honeycomb sandwich structure and stiffened panels.

This paper describes the design, ground tests, and flight test of the HondaJet with particular emphasis on these advanced technologies.

2 General Arrangement and Performance

The general arrangement is shown in Figure 2. The aircraft is powered by two Honda HF-118 fuel-efficient turbofan engines, each rated at 1,670 lb thrust at takeoff power (Fig. 3). The engine is controlled by the Full Authority Digital Engine Control (FADEC) system. The aircraft is a low-wing configuration with the engines mounted over the wing. The aircraft is 41.14 ft long, has a wing span of 39.87 ft, and is 13.21 ft high at the top of the T-tail. Design maximum takeoff weight is about 9200 lb. The estimated maximum speed is about 420 knots at 30,000 ft and the maximum range is about 1100 nm. The aircraft provides a very large cabin volume compared to those of other four-passenger seat arrangements and it is also possible to add two more passenger seats without sacrificing comfort. The cabin is pressurized up to 8.7 psi to maintain an 8,000-ft cabin altitude up to 44,000 ft.

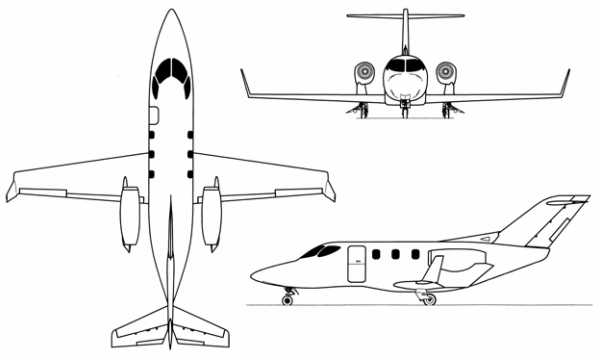

Fig. 2. General arrangement.

Fig. 3. HF-118 turbofan engine.

3 Aerodynamic Design

3.1 Over-the-wing Engine-Mount Configuration

Engine location was the major design decision in the development of the HondaJet configuration. In general, locating the engine nacelles over the wing causes unfavorable aerodynamic interference and induces a strong shock wave that results in a lower drag-divergence Mach number. Theoretical studies were conducted using a three-dimensional Euler solver [3],[4] to investigate this configuration (Fig. 4). A transo-

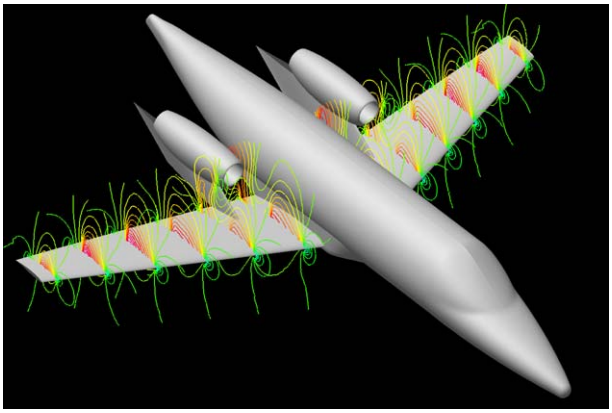

Fig. 4. Off-body pressure contour of the OTWEM configuration.

nic wind-tunnel test (Fig. 5) was conducted in the Boeing Transonic Wind Tunnel (BTWT) to validate the theoretical predictions. It was found that the shock wave is minimized and drag divergence occurs at a Mach number higher than that for the clean-wing configuration when the nacelle is located at the optimum position relative to the wing. The over-the-wing engine-mount configuration exhibits lower drag than does the conventional rear-fuselage engine-mount configuration[1]. The final aircraft configuration is based on this result. By employing this optimum over-the-wing engine-mount configuration, the cruise efficiency is higher than that of a conventional rear-fuselage engine-nacelle configuration and, in addition, the cabin volume is maximized.

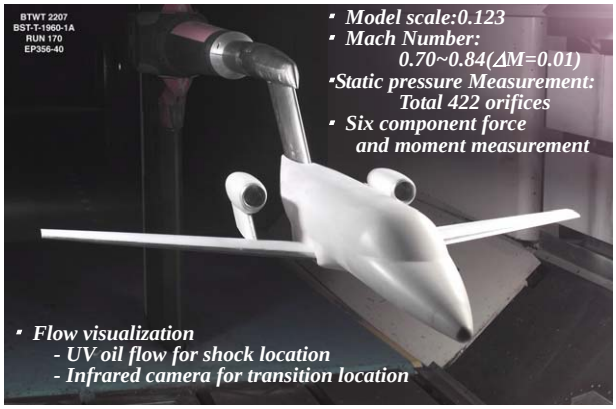

Fig. 5. Transonic wind tunnel test model (BTWT).

3.2 Wing

The main goal for the aerodynamic design of the wing is to achieve minimum drag while maintaining good stall characteristics. Detail design studies were performed to minimize the induced drag with minimum wing weight. The study showed that the takeoff weight is minimized for a 1100-nm-range aircraft when the wing geometric aspect ratio is 8.5 and a winglet having a height of 9-percent of the wing span is installed. Because of the over-the-wing engine-mount configuration, the stall characteristics were carefully studied by theoretical analysis and low-speed wind-tunnel tests. From the theoretical analysis using a vortex-lattice method combined with a critical-section method, which was developed by the author, and a three-dimensional, panel method [5],[6] combined with the pressure-difference rule [7], a taper ratio of 0.38 and a washout of 5.1 degrees were chosen to provide good stall characteristics with minimum induced drag penalty. The stall pattern of the over-the-wing engine-mount configuration obtained from a 1/6-scale, low-speed wind-tunnel test is shown in Figure 6. The wing stalls first around 55-percent semi-span. The separation propagates inboard, although the root region of the wing between the fuselage and the nacelle is not stalled at the aircraft stall angle of attack. Thus, the over-the-wing engine-mount configuration exhibits good stall characteristics. In addition, there is adequate stall margin over the outboard portion of the wing. The lift curves obtained from the 1/6-scale test with and without nacelles are shown in Figure 7. The zero-lift angle of the over-the-wing engine-mount configuration is about 1.2 degrees higher than that of the clean-wing configuration. The maximum lift coefficient of the over-the-wing engine-mount configuration is about 0.07 higher than that of the clean-wing configuration. Thus, there is no disadvantage with respect to the lift characteristics due to the nacelle installation over the wing.

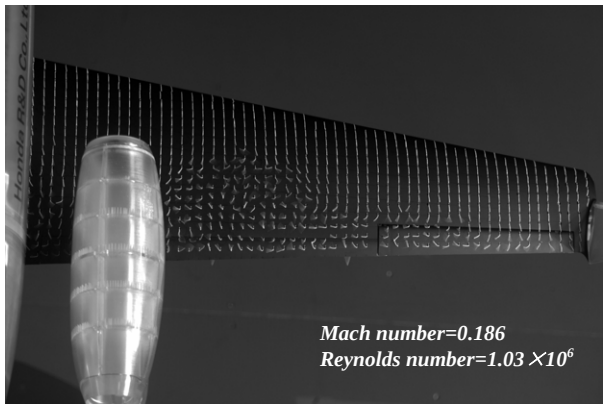

Fig. 6. Stall pattern.

To satisfy the requirements of the HondaJet, a new natural-laminar-flow airfoil, the SHM-1, was designed using a conformal-mapping method [8]. The pressure gradient on the upper surface is favorable to about 42-percent chord, followed by a concave pressure recovery, which represents a compromise between maximum lift, pitching moment, and drag divergence. The

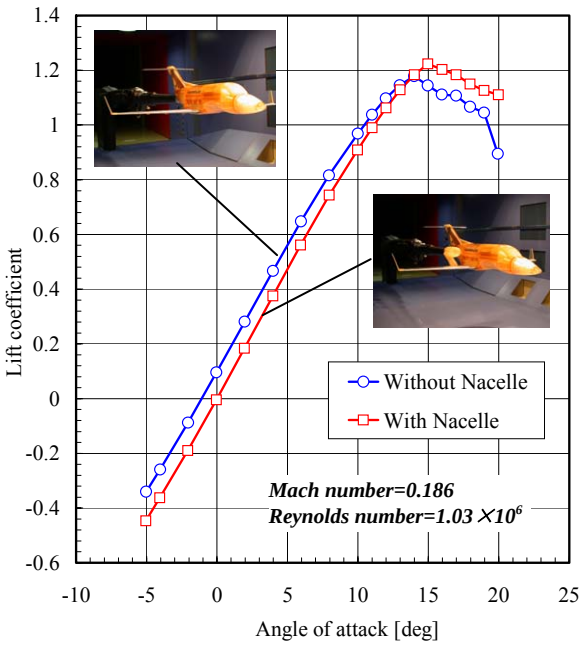

Fig. 7. Comparison of lift curve with and without nacelle configuration.

pressure gradient along the lower surface is favorable to about 63-percent chord to reduce drag. The leading-edge geometry was designed to cause transition near the leading edge at high angles of attack to minimize the loss in maximum lift coefficient due to roughness. The upper-surface trailing-edge geometry was designed to produce a steep pressure gradient and, thereby, induce a small separation. By the incorporation of this new trailing-edge design, the magnitude of the pitching moment at high speeds is greatly reduced [2]. The shape of the SHM-1 airfoil and an example of the pressure distribution are shown in Figure 8. The airfoil has been tested in low-speed and transonic wind-tunnels. In addition, a flight test using a gloved T-33 aircraft (Fig. 9) was conducted to validate the performance of the airfoil at full-scale Reynolds number and Mach number. The airfoil exhibits a high maximum lift coefficient with docile stall characteristics and low profile-drag coefficients in cruise and climb.

3.3 Engine Simulator Test for OTWEM Configuration

It is important to investigate the inlet-flow distortion at high angles of attack especially for

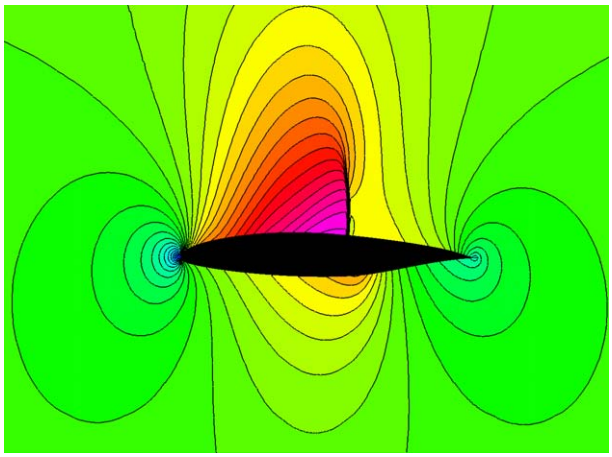

Fig. 8. SHM-1 airfoil shape and pressure contour.

Fig. 9. T-33 aircraft modified for NLF flight test.

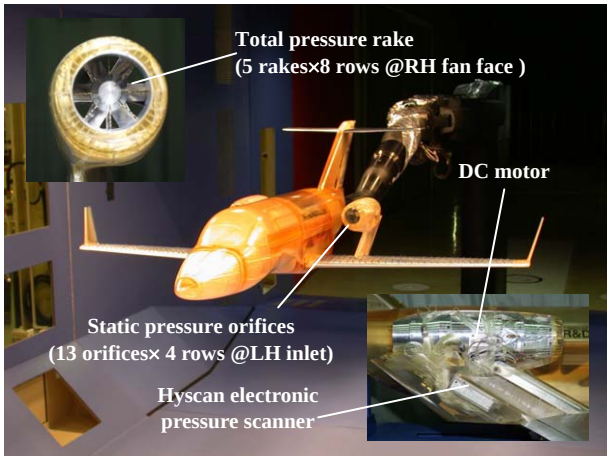

Fig. 10. 1/6-scale engine simulator.

the over-the-wing engine-mount configuration. To evaluate these characteristics, a 1/6-scale, powered-model test using DC motor engine simulators was conducted in the Honda Low-Speed Wind Tunnel (Fig.10). An investigation was conducted to determine if the measured total-pressure distortion exceeded the limits for high and low mass-flow conditions at

various angles of attack and sideslip angles. Examples of the distortion pressure patterns at four angles of attack (10, 15, 18, and 26 degrees) and three sideslip angles (-18, 0, and 18 degrees) with a mass-flow ratio of 1.15, which corresponds to approach speed at required thrust, are shown in Figure 11. The inlet total-pressure distortion is less than 0.1 percent up to the stall angle of attack of 15 degrees and less than 2 percent up to a post-stall angle of attack of 26 degrees. Similar tendencies were obtained from tests with mass-flow ratios of 0.65 and 2.15. The results demonstrate that the distortion does not exceed the limits specified by engine requirements within the flight envelope.

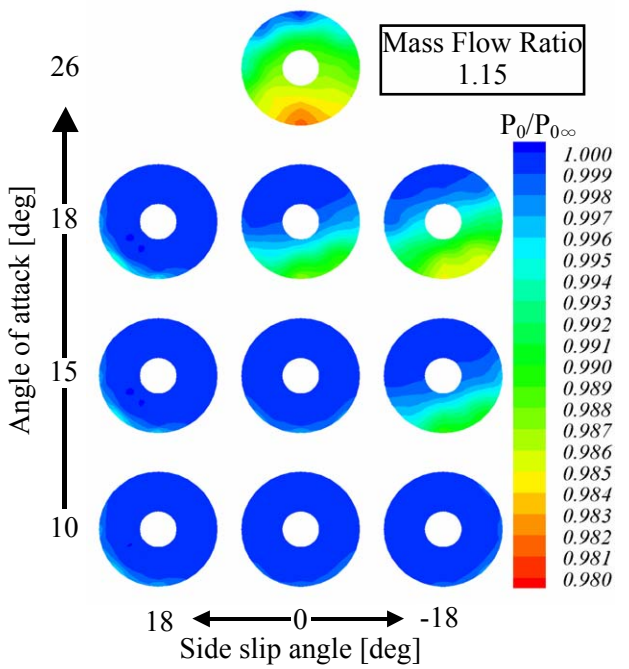

Fig. 11. Pressure distribution pattern obtain from powered model test.

3.4 Natural-Laminar-Flow Fuselage Nose

A natural-laminar-flow, fuselage-nose shape was developed through extensive analysis and experiments to reduce the fuselage drag. Using a three-dimensional, panel code with an integral boundary-layer method [5], [6], the fuselage-nose contours were designed to maximize laminar -flow length by maintaining a favorable pressure gradient and minimizing crossflow instabilities. A 1/3-scale test was conducted in the Honda Low-Speed Wind Tunnel to validate the design (Fig. 12). The streamlines on the nose were visualized using the oil-flow technique (Fig. 13) and the observed patterns were compared to those from the theoretical analysis [5], [6]. The infrared technique was also used to visualize the laminar flow on the nose at each angle of attack (Fig. 14). The results show that extensive laminar flow is achieved at climb and cruise angles of attack. Because steps and gaps have a detrimental effect on the achievement of laminar flow (e.g., [9]), various steps and gaps were installed on the nose to determine the critical dimensions. By employing a natural-laminar-flow nose, the fuselage drag is reduced about 10 percent compared to that of a turbulent-flow nose fuselage.

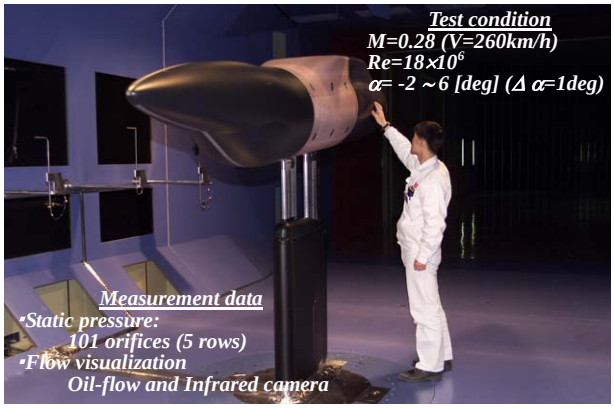

Fig. 12. 1/3-scale fuselage model for NLF nose test.

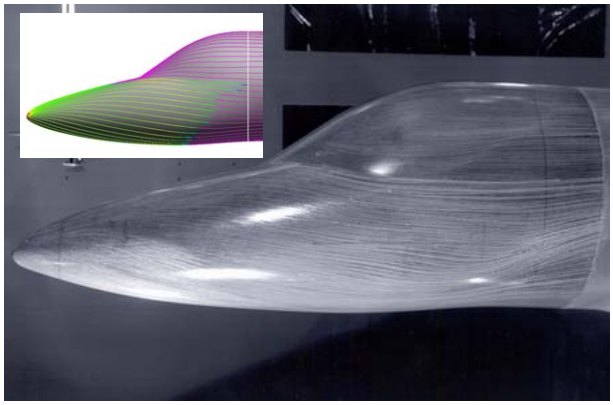

Fig. 13. NLF nose flow pattern.

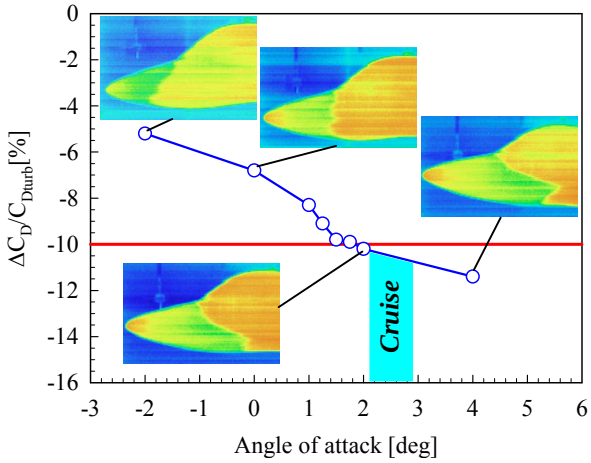

Fig. 14. Drag reduction of NLF nose.

3.5 High-Lift System

A 30-percent-chord, double-slotted flap, which is deployed by a mechanical linkage, is employed to satisfy the stall-speed requirement as well as the high-speed requirement. The position of the vane with respect to the flap is fixed. The shapes of the vane and the flap as well as the gap and overlap were designed using a two-dimensional, multielement, panel code (MCARFA, [10]) and a two-dimensional, multielement, Euler code (MSES, [11]). The flap and vane shapes and positions were then tested on a 1/3-scale, half-span model in the Honda Low-Speed Wind Tunnel (Fig. 15) and the results were compared with those from analysis (Fig.16) using a three-dimensional panel code [5], [6]. A test was also conducted using a 1/6-scale model in the Honda Low-Speed Wind Tunnel. Examples of the lift curves obtained from the 1/3-scale and 1/6-scale tests are shown in Figure 17. The results for two Reynolds numbers allowed the full-scale maximum lift coefficient to be estimated more accurately using an analytical method that incorporated the pressure-difference rule [7]. The maximum lift coefficient for the full-scale Reynolds number is estimated to be higher than 2.5, which satisfies the stall-speed requirement.

3.6 Wind Tunnel Test

Low-speed wind-tunnel tests were conducted to obtain the aerodynamic characteristics of the aircraft. Two different wind tunnels, the

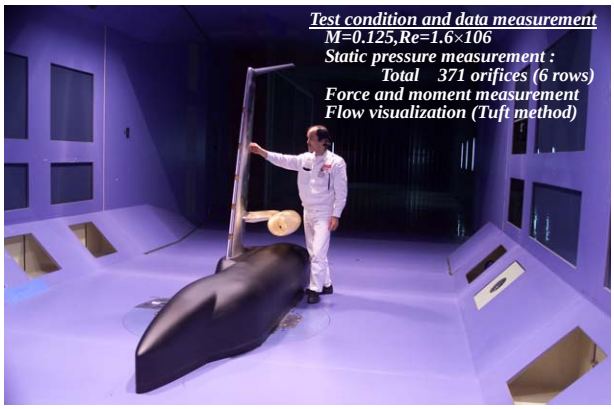

Fig. 15. 1/3-scale low-speed wind tunnel test model.

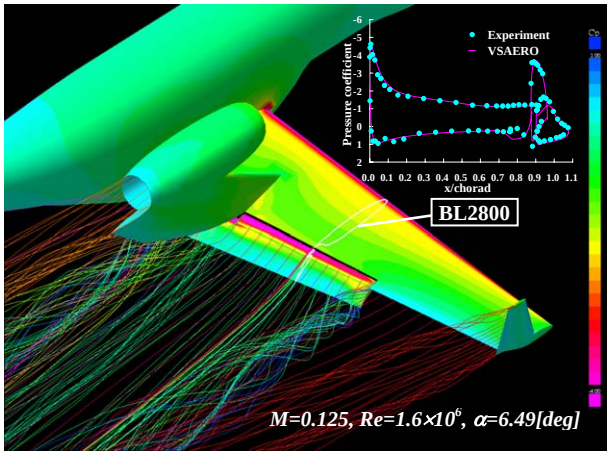

Fig. 16. Experimental and Theoretical Pressure Distribution of Flap.

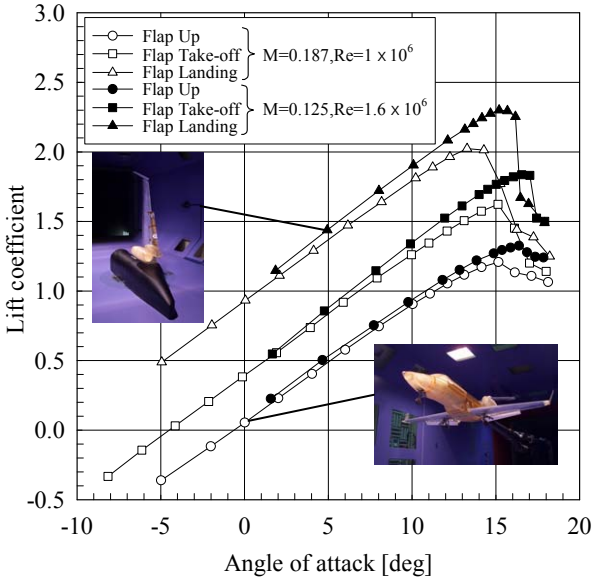

Fig. 17. Lift curves with high lift device.

Honda Low-Speed Wind Tunnel (Fig. 18(a)) and the University of Washington (UW) low-speed wind tunnel (Fig. 18(b)) were used.

The stability derivatives obtained from these tests were used to evaluate the flight characteristics. The tests were conducted to very high angles of attack to obtain the post-stall aerodynamic characteristics of the aircraft, which are critical for a T-tail configuration.

(a) Honda Low-speed wind tunnel

(b) UW low-speed wind tunnel

Fig. 18. 1/6-scale wind tunnel.

3.7 Flight Simulator

To evaluate the flying qualities of the aircraft, a flight simulator, called the Honda Nonlinear Aerodynamics Flight Simulator (HNAFS), was developed (Fig. 19). The simulator solves the six-degree-of-freedom equations of motion in real time. The stability derivatives for the equations of motion were interpolated for each angle of attack, sideslip angle, control-surface deflection, etc., from an aerodynamic database developed from the wind-tunnel test results. By interpolating within the database, the HNAFS accurately simulates not only normal flight conditions but also critical flight conditions such as deep stall, spin, and one-engine out. A special feature of the HNAFS is the dynamic spin-chute model, including the inflation process, which was developed by the author. The deep-stall characteristics, which are especially critical for a T-tail aircraft (e.g., [12]), were carefully evaluated using the HNAFS. An example of a deep-stall recovery simulation using a spin chute is shown in Fig. 20. The time histories of the aircraft angle of attack and the elevator deflection are shown in Figure 20(a) and the time history of the riser tension, in Figure 20(b). This simulation shows that the aircraft can be recovered from deep stall with a spin chute under emergency conditions. The simulation results were also used to design the support structure for the spin chute.

Fig. 19. Honda flight simulator (HNAFS).

4 Aeroelasticity

The flutter characteristics of the over-the-wing engine-mount configuration were investigated through extensive theoretical studies and wind-tunnel tests. The location of the engine mass and the stiffness of the pylon relative to that of the wing are important for wing-flutter characteristics. Theoretical analysis using the ERIN code [13], which was developed by the author, was performed. Low-speed and transonic wind-tunnel flutter tests (at the National Aeronautical Laboratory Transonic Flutter Wind Tunnel) were then conducted to validate the design (Fig. 21). The study shows that the symmetric flutter mode is more critical than the anti-symmetric mode for the over-the-wing engine-mount configuration.

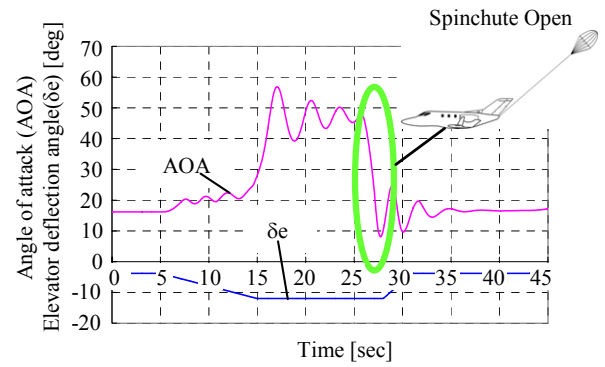

(a) Time history of the aircraft AOA and δe.

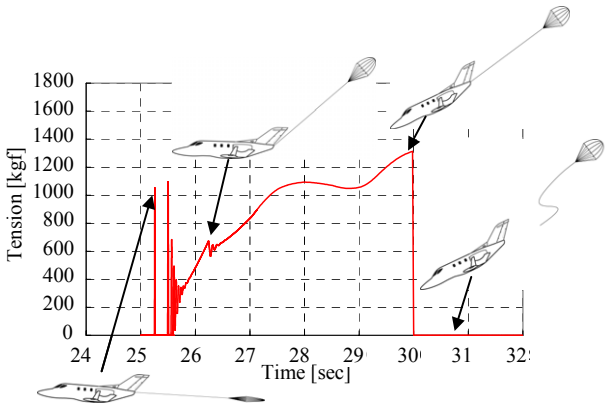

(b) Time history of the riser tension.

Fig. 20. Deep stall simulation with spinchute deployment.

Fig. 21. Transonic wind tunnel flutter test at NAL transonic wind tunnel.

Also the effects of the aerodynamic load and the interference due to the engine-nacelle installation over the wing are small for this over-the-wing engine-mount configuration. In addition, the engine-pylon vibration characteristics influence the flutter characteristics. The flutter speed is highest when the engine-pylon side-bending frequency is close to the uncouple 1st wing-torsion frequency (about 0.9 to 1.0 times the uncouple 1st wing-torsion frequency). The flutter speed is lowest when the engine-pylon pitching frequency is about 1.25 times the uncouple 1st wing-bending frequency [13]. Based on these results, the wing stiffness and mass distributions were designed to satisfy the flutter-clearance requirements.

5 Structure

5.1 Wing

The wing is metal and constructed in three sections: the left outboard wing, the center section, and the right outboard wing (Fig. 22). The torque box contains three spars, the ribs, and the skin with integrated stringers forming an integral fuel tank. The upper skin is a machined, integral panel to maintain the contour required by laminar flow. By using integral, machined panels, the material can be distributed in the most efficient manner and the number of parts is minimized. The leading-edge structure and the main torque-box structure are mated at about 13.5-percent chord to reduce the disturbance to the laminar flow. The leading edge is equipped with an anti-ice system that uses engine bleed air ejected through a piccolo tube that directs the hot air against the inside of the leading-edge skin. The pylon structure is attached to a rein-

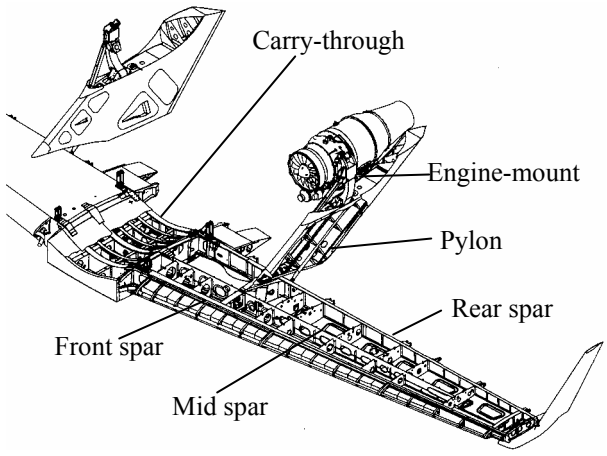

Fig. 22. Wing structure.

forced wing rib by four bolts. The main landing gear is also attached to the inboard end of the same reinforced rib to concentrate the heavy loads in one reinforced structure. The wing is mounted under the fuselage by four links and two thrust rods. The vertical loads are transmitted to the front- and rear-fuselage main frames by the links and the lateral loads are transmitted by the V-shaped links. The drag loads are transmitted to the fuselage by the two thrust rods.

5.2 Fuselage

The fuselage is constructed entirely of graphite composites. The material is a 350-degree-F cure epoxy prepreg reinforced by carbon fiber. (The matrix is Cytec 5276-1 high-damage-tolerance, epoxy resin and the reinforcement is TOHO G30-500 high-strength, intermediate-modulus fiber.) As shown in Figure 23, the cockpit as well as the tail section is a honeycomb sandwich construction to maintain the compound curves, which are especially important for the laminar-flow nose. An integrally stiffened panel structure is employed for the constant cross-section portion of the cabin, which maximizes the cabin volume [14]. The frames and stringers have identical dimensions in the constant cabin section so the number of molds for the frames and stringers are minimized. The constant fuselage section can be easily extended to satisfy future fuselage stretching. A feature of the fuselage fabrication is that the sandwich panel and the stiffened panel are co-cured integrally in an autoclave to reduce weight and cost. It was a technical challenge to cure the honeycomb sandwich structure under the pressure (85.3 psi) required for the stiffened panel but a new method called the "picture-frame stabilizing method" prevents core crushing.

The aircraft employs compound-curved windshields to obtain better aerodynamic characteristics. The windshields are two plies (outer and inner) of stretched acrylic material with a polyurethane interlayer, which has superior low-temperature ductility, a higher allowable operating temperature, and higher adhesive properties. The outer surface of the outer acrylic ply and the inner surface of the inner acrylic ply are hard coated for abrasion and chemical resistance. The windshield is electrically heated for anti-ice protection. The windshield and its support structure were designed to withstand the impact of a four-pound bird strike at Vc (structural design speed) at sea level.

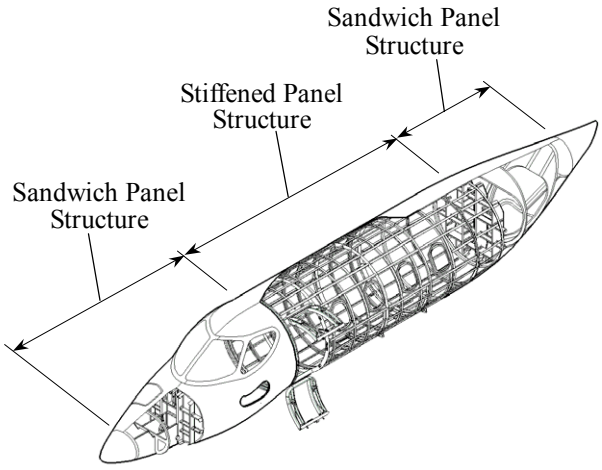

Fig. 23. Fuselage structure.

5.3 Empennage

The empennage is a T-tail configuration. The horizontal tail is a conventional, two-spar, aluminum structure. The fin is also a conventional, two-spar structure. The front spar of the fin is, however, joined to the fuselage by a pin support and transmits only the forward, vertical, and lateral loads to the fuselage. The rear spar is cantilever mounted to the rear-fuselage canted frame and transmits all bending moments to the fuselage. The fin first torsion frequency is very critical for the T-tail flutter mode and, therefore, relatively heavy-gauge skin (0.04 in.) was employed to provide adequate torsional stiffness. Shear buckling is not allowed up to the limit-load condition to prevent torsional-stiffness reduction.

6 Systems

6.1 Landing Gear

The landing gear is a typical tricycle-type layout with a steerable nose wheel.

The nose gear is of the shock-absorber strut type. It is retracted forward by a drag-brace actuator (Fig. 24). The doors are mechanically linked and open and close automatically with nose -gear movement. The drag-brace actuator has an internal down-lock mechanism. The nose gear is equipped with a steer-by-wire system that is electrically controlled and hydraulically actuated. There are two modes for the steering system: parking mode, in which the steering-angle range is +/-50 degrees, and normal mode, in which the steering angle is limited to +/-10 degrees. Accumulator pressure provides emergency steering control should the hydraulic pump fail.

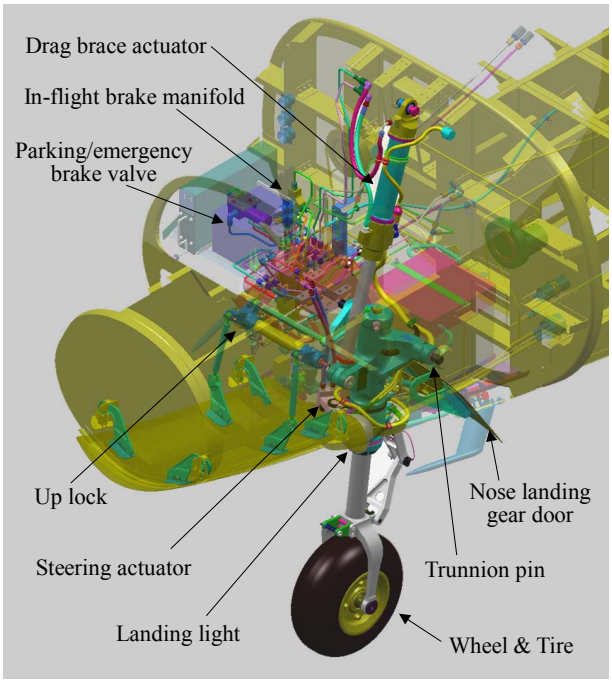

Fig. 24. Nose landing gear.

The main landing gear is of the trailing-link type and attached to the main wing (Fig. 25). A side-brace actuator is used to extend and retract the landing gear. The landing-gear doors consist of three separate doors: inboard, middle, and outboard. The inboard door is operated by an independent hydraulic actuator and the middle and outboard doors are linked to the main-gear strut and open and close automatically with main-gear movement. The wheel well is completely covered by the doors and, therefore, the tires are not exposed during cruise thus reducing drag. The side-brace actuator is equipped with an internal down-lock mechanism. Under emergency conditions, opening a dump valve and releasing the up-lock mechanism by manual cable allow the free-fall extension of the gear.

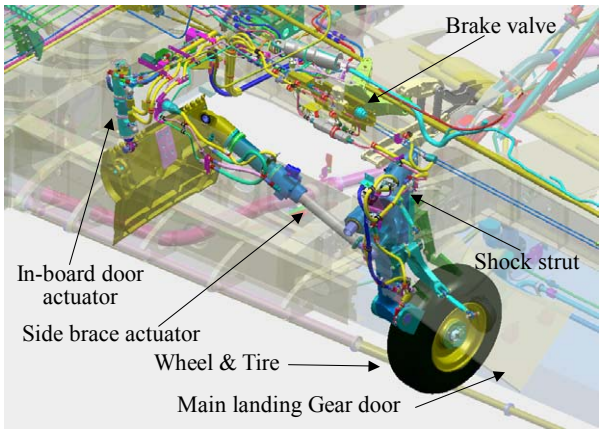

Fig. 25. Main landing gear.

The main gear is equipped with an anti-lock braking system. A dynamometer test was conducted to optimize the anti-lock system control. Locked-wheel protection, touch-down protection, and spin-up override are also incorporated into the braking system.

Drop tests were conducted and the shock-absorption characteristics evaluated. The main landing gear and the nose gear were dropped with a weight simulating the aircraft weight (Fig. 26). The results showed that the efficiency of the oleo shock satisfies the requirement.

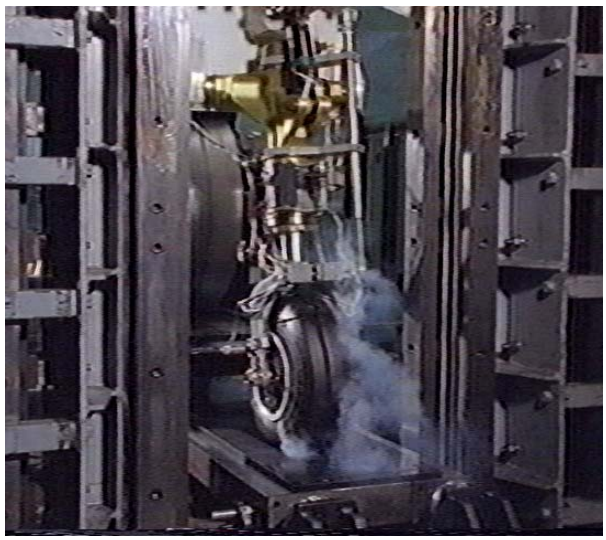

Fig. 26. Nose landing gear drop test.

6.2 Flaps

A linkage mechanism is used for the flap system. The flap system has two positions: 15.7 degrees down for takeoff and 50 degrees down for landing, as shown in Figure 27. The flap is deployed by two hydraulic actuators: one for the right wing and the other for the left, each installed at the wing root (Fig. 28). The right and left flaps are mechanically interconnected to prevent a split condition.

A flap-mechanism fatigue test as well as a strength test were conducted. Simulated airloads were applied by a whiffle tree pulled by a hydraulic actuator. For the fatigue test, the hydraulic actuator moves with flap movement such that the loads are continuously applied as in the flight condition. The flap mechanism satisfies the strength and fatigue-cycle requirements determined for the flight-test program.

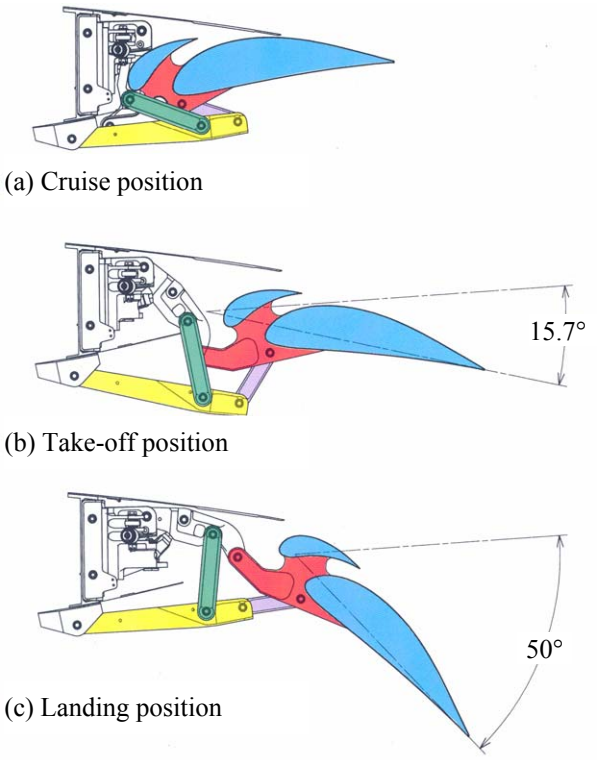

(a) Cruise position

(b) Take-off position

(c) Landing position

Fig. 27. Flap linkage mechanism.

6.3 Fuel

There are four fuel tanks in the aircraft: a right-wing integral tank, a left-wing integral tank, a carry-through tank, and a rear-fuselage bladder tank, as shown in Figure 29. The aircraft is refueled from a single point located on the right side of the rear fuselage. The fuel is transferred from the carry-through tank to the right- and left-wing integral tanks by transfer pumps located in the carry-through tank. The right-wing tank feeds the right engine and the left-wing tank feeds the left engine through collector tanks located under each pylon. The primary pumps are ejector-type units and electric boost pumps are used to provide fuel pressure for engine starting and cross feed. The Fuel Transfer Management Unit (FTMU) maintains the fuel level in the wing, which relieves the average wing-root bending moment as much as 12 percent. An automatic cross-feed function is incorporated to correct fuel imbalance between the left and right wings. A total of 13 capacitance-type fuel probes--three in the carry-through tank, two in the bladder tank, and four in each wing tank--are provided. The fuel quantity can be measured within an

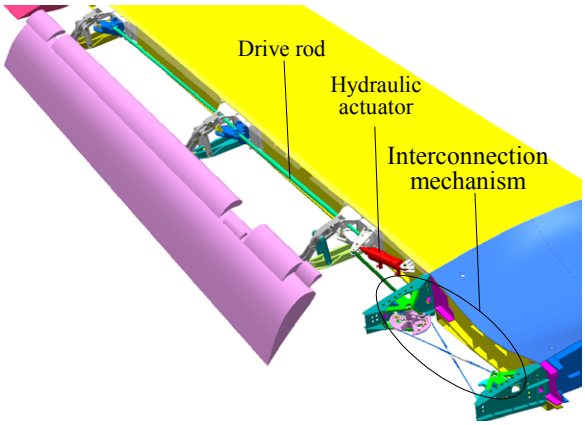

Fig. 28. Flap system.

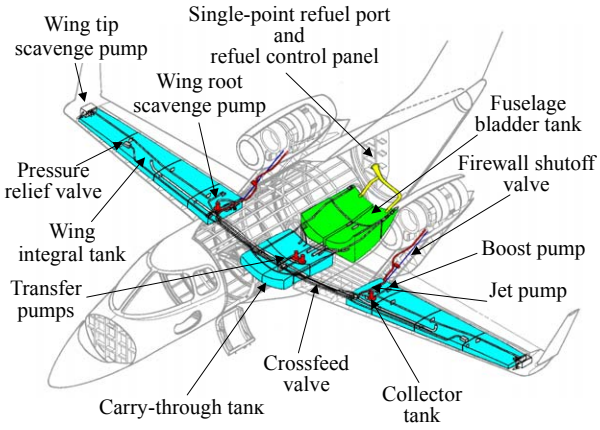

Fig. 29. Fuel system.

Fig. 30. Cockpit.

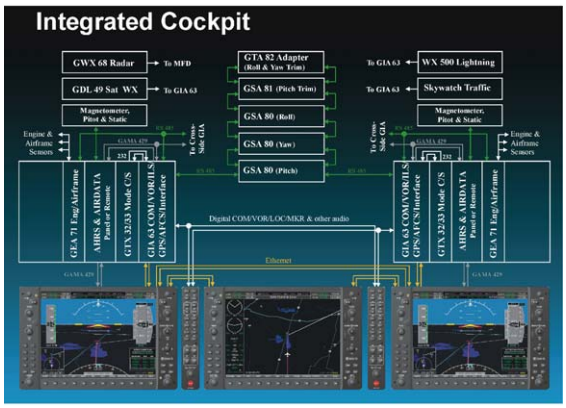

Fig. 31. Avionics system.

accuracy of 2 percent of the indicated fuel quantity plus 1 percent of full scale during sustained flight conditions anywhere in the normal flight envelope.

6.4 Avionics

The aircraft employs a Garmin all-glass flightdeck, which is a modular design having open architecture. The cockpit is shown in Figure 30. All information--from flight and engine instrumentation to navigation, communi-cation, terrain and traffic data, etc.--is uniquely integrated and digitally presented on the dual, large-format, high-resolution Primary Flight Displays (PFD) and the Multi-Function Display (MFD). The PFD contains the airspeed indicator, vertical-speed indicator, adjustable altimeter, direction indicator, pitch and bank indicator (artificial horizon), slip/skid indicator, dual NAV/COM, etc. and the MFD contains the EIDS (N1, ITT, N2, oil temperature and pressure), fuel flow, fuel quantity, generator current, GPS map, etc. The system diagram is shown in Figure 31. This cockpit configuration provides a high degree of integration for enhanced situational awareness, functionality, ease of operation, redundancy, and flight safety.

7 Ground Tests

7.1 Structural Proof Test for Wing and Fuselage Structures

Proof tests were conducted to substantiate the structural design of the wing (Fig. 32) and fuselage (Fig. 33). The MTS Aero-90 test system (Fig. 34) was used to apply loads. A

Fig. 32. Wing proof test.

Fig. 33. Fuselage proof test.

total of 26 computer-controlled actuators were used to apply the simulated airloads, engine loads, landing-gear loads, etc. More than 600 channels of data (e.g., strain, displacement, and force) were measured and monitored at each test condition. A total of 10 load cases out of 870 were evaluated for the wing proof test (pylon vertical load, pylon side load, flap load, Vc positive gust, Vc negative gust, right-hand and left-hand one-gear landing conditions, level landing with spin-up load, side landing, and

rudder maneuver). A total of 6 load cases out of 1275 were evaluated for the fuselage test (pressurization load, positive-gust load, positive -gust load with pressurization, rudder-maneuver load, rudder-maneuver load with pressurization, and two-point landing load). Because the structures used for these tests were also used for the flight-test program, the test loads were limited to 80 percent of the limit loads. The measured strain, displacement, and reaction-force data were compared with those from a finite-element analysis and the results were used to evaluate the limit-load condition.

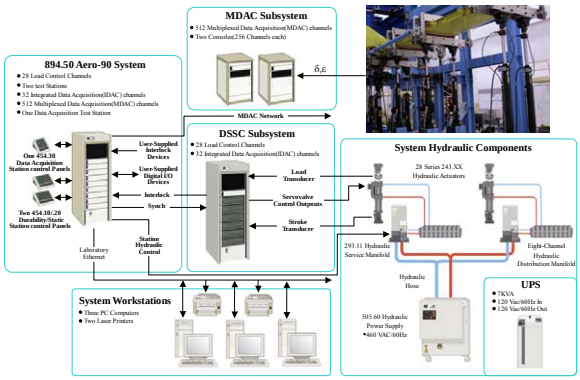

Fig. 34. MTS Aero-90 system.

Fig. 35. Empennage proof test.

7.2 Static Test of Empennage Structure

A component strength test was conducted to validate the structural design of the empennage up to the ultimate load. The distributed loads were applied to the structure through tension pads and a whiffle tree (Fig. 35). A dummy rear fuselage, which simulates the actual structure, was used to evaluate the joint structure. The empennage took the limit load without permanent deformation and the ultimate load without any damage. Also the fin bending and torsion-stiffness distribution were measured; there is no shear buckling up to the limit-load condition.

7.3 Control-System Proof Test

The HondaJet has dual flight controls with column-mounted control wheels and adjustable rudder pedals. A combination of cable and push-pull rod mechanisms is used to actuate the elevator system and a cable mechanism is used for the rudder and aileron systems. A proof test was conducted to validate the elevator, rudder, and aileron control-system designs (Fig. 36(a)). Control-system deflection under the limit load

(a) Test set up

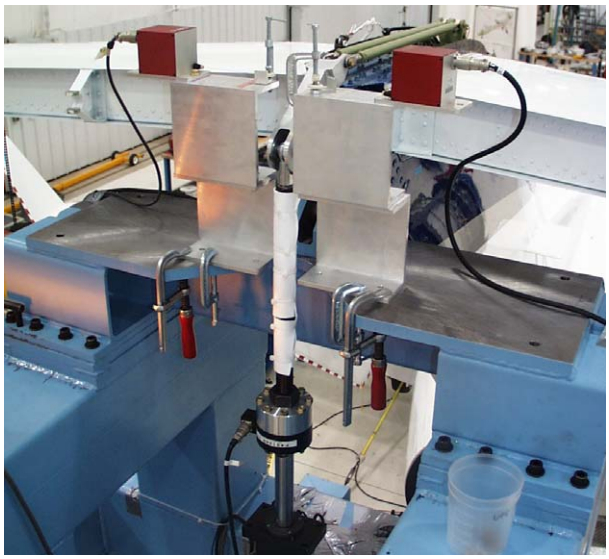

(b) Hydraulic actuator

Fig. 36. Control system proof test.

and breakout force were also measured. Loads were applied to the control surface by a hydraulic actuator (Fig. 36(b)) and the control column or the rudder pedal was fixed by another actuator. Control-system stiffness and friction force were evaluated and the system mechanism was adjusted to satisfy the requirement.

7.4 Ground Vibration Test (GVT)

A ground vibration test was conducted to measure the vibration modes of the entire aircraft and to establish the correlation with those from the finite-element vibration analysis. The aircraft was excited by six electrodynamic shakers, which were attached to the aircraft by flexible rods. The structural responses were measured by a total of 383 piezoelectric accelerometers attached to the aircraft (Fig. 37). The ground vibration system is shown in Figure 38. The Maximum Entropy Method (MEM) was used to identify the modal parameters. The advantage of the MEM is that it provides higher frequency resolution with smaller frame size compared to classical FFT methods because the frame size and the number of spectra lines are independent of each other. The aircraft was placed on specially designed air springs, which decouple the rigid mode of the aircraft (Fig. 39). The finite-element model was tuned by using the frequencies and mode shapes measured from the ground vibration test to accurately determine the aeroelastic characteristics of the aircraft.

Fig. 37. Ground Vibration Test.

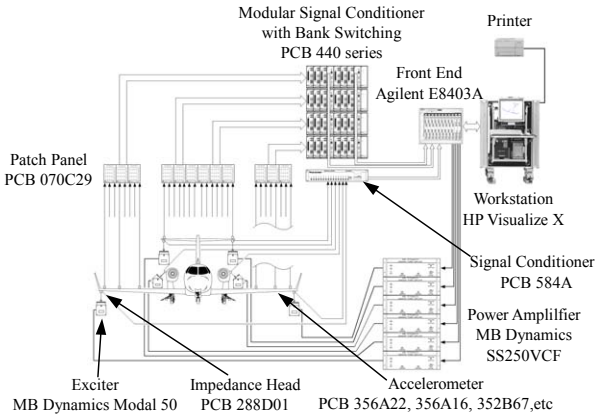

Fig. 38. Block diagram of GVT system.

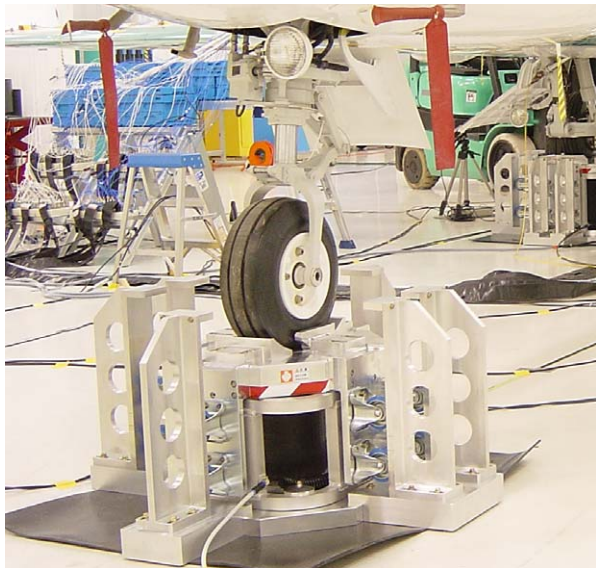

Fig. 39. Air spring.

7. 5 Taxi Test

Taxi tests were conducted to evaluate braking and steering performance (Fig. 40). It is important to evaluate the heat-sink capacity of the braking system because a very large amount of heat is generated during braking. An example of the brake-temperature measurement for each barking speed is shown in Figure 41. The temperature is close to the estimates and the result validates the brake heat-sink capacity. The shimmy characteristics were also evaluated and the measured damping satisfies the requirement.

The acceleration and stopping distances were measured and compared to those from analysis. An example of acceleration and stopping-distan-

ce measurement is shown in Figure 42. The brake pressure applied for these tests were from 60 to 100-percent of the maximum pressure. The measured distances fall within the range of analyses for friction coefficients from 0.30 to 0.40.

Fig. 40. High-speed taxi test.

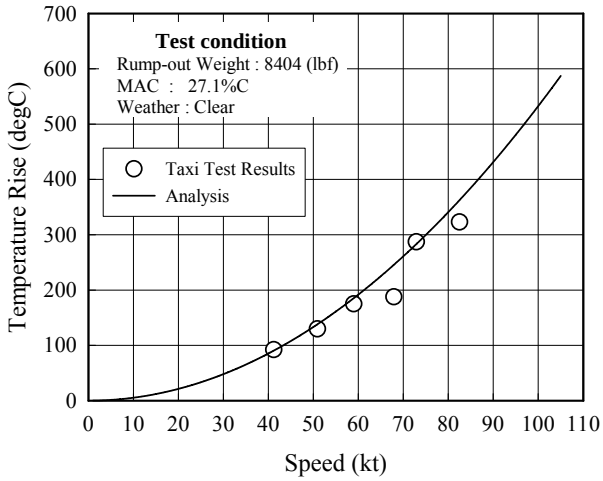

Fig. 41. Brake disk temperature rise vs taxi speed.Fig.

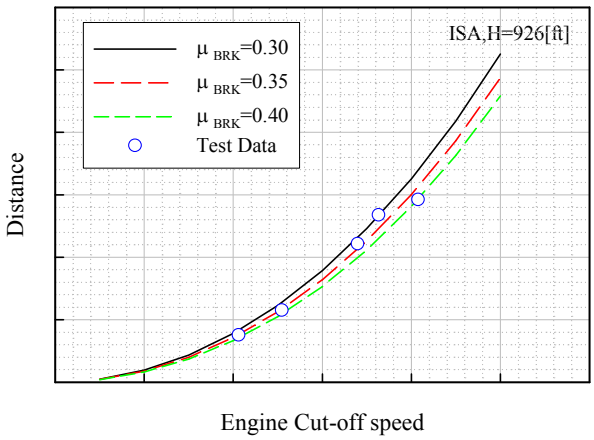

Fig. 42. Accelerate-stop distance.

8 Flight Test

After the ground tests were completed, the first flight was performed on December 3, 2003, at the Piedmont Triad International Airport in North Carolina. The flight-test program began in January 2004 (Fig. 43).

The prototype is fully instrumented with a data-acquisition system and a telemetry system to maximize the efficiency of the flight-test program (Fig. 44). More than 200 sensors, which measure air data, attitude, acceleration, control-surface deflection and control force, etc., are installed on the aircraft and all data are transmitted to the ground. The data are analyzed in real time on the ground [15].

In phase one of the flight-test program, in-flight system-function tests such as landing-gear and flap operation were conducted. The tests were performed under different flight conditions (e.g., airspeed, sideslip angle, etc.) and the function was confirmed. Emergency gear operation was also conducted to validate the extension of the landing gear simulating electrical- and hydraulic-system failure.

In phase two, stability-and-control and performance tests were conducted. Static and dynamic stability, such as short-period, phugoid, and dutch-roll modes, were evaluated by measuring the undamped natural frequencies and damping ratios at various flight conditions. Cruise performance was evaluated by the speed-power method. The results were compared to analytical estimates and good agreement was found.

Fig. 43. HondaJet flight test.

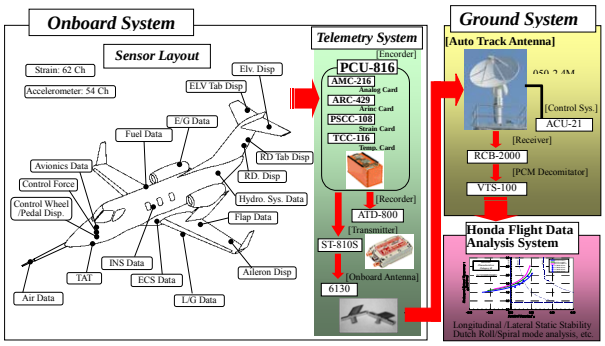

Fig. 44. Telemetry block diagram.

9 Concluding Remarks

Honda R&D is developing an advanced, lightweight, business jet. The challenge of employing an unconventional configuration--an over-the-wing engine-mount configuration with natural-laminar-flow wing and fuselage nose, composite fuselage, etc.--has been met. Extensive analyses and ground tests have been conducted to validate the design. Flight tests are being performed and the results are promising. More detailed performance tests as well as critical tests, such as flutter, will be conducted in the next phases of the flight-test program.

10 References

[1] Fujino, M. and Kawamura, Y., "Wave-Drag Characteristics of an Over-the-Wing Nacelle Business-Jet Configuration." Journal of Aircraft, Vol.40, No.6, November-December 2003, pp1177-1184

[2] Fujino, M., et al., "Natural-Laminar-Airfoil Development for a Lightweight Business Jet," Journal of Aircraft, Vol. 40, No.4, July-August 2003, pp609-615

[3] Strash, D. J.; and Tidd, D. M.: MGAERO User's Manual. Analytical Methods, Inc. Redmond, Washington, 2002

[4] Tidd, D. M.; et al.: Application of an Efficient 3-D Multi-Grid Euler Method to Complete Aircraft Configurations. 9th AIAA Applied Aerodynamics Conference, AIAA Paper 91-3236, Baltimore, MD, Sep. 1991.

[5] Maskew, B.: Prediction of Subsonic Aerodynamic Characteristics: A Case for Low-Order Panel Methods. J. Aircraft, vol. 19, no. 2, Feb. 1982.

[6] Nathman, James K.: VSAERO User's Manual Version 6.3. Analytical Methods, Inc. , Redmond, Washington, June 2001.

[7] Valarezo, W. O., and Chin, V. D., "Maximum Lift Prediction for Multielement Wings" AIAA Paper 92-0401, Jan. 1992.

[8] Eppler, Richard: Airfoil Design and Data. Springer-Verlag (Berlin), 1990.

[9] Holmes, Bruce J.; et al.: Manufacturing Tolerances for Natural Laminar Flow Airframe Surfaces. 850863, Soc. Automot. Eng., Apr. 1985.

[10] Morgan, Harry L.: High-Lift Flaps for Natural Laminar Flow Airfoils. Laminar Flow Aircraft Certification, NASA CP-2413, 1986, pp. 31-65.

[11] Drela, M.: Design and Optimization Method for Multi-Element Airfoils. AIAA Paper 93-0969, Feb. 1993.

[12] Fujino, M., "Aerodynamic and Aeroelastic Design of Experimental Aircraft MH02, " DOT/FAA/CT-94/63 Proceedings of the 1994 AIAA/FAA Joint Symposium on General Aviation Systems, May 24-25, 1994, pp. 435-459.

[13] Fujino, M.; et al.: Flutter Characteristics of an Over-the-Wing Engine Mount Business-Jet Configuration. AIAA Paper 2003-1942, Apr. 2003.

[14] Matsui, N.; and Sato, K.: Research Work of the All-Composite Fuselage. Proceedings of 14th International Conference on Composite Materials, July 2003.

[15] Fujino, M.; et al.: Flight Test of the HondaJet. ICAS 2004-4.10.1, Proceedings of the 24th Congress of the International Council of the Aeronautical Sciences, August 29 -September 3, 2004

11 Acknowledgements

The author wishes to thank Honda R&D for permission to publish this paper and my colleagues for their invaluable assistance. The author also wishes to gratefully acknowledge the cooperation of GARMIN International in the development of the avionics system and Sumitomo Precision Products in the landing-gear development. Finally the author would like to thank Atlantic Aero for their cooperation in this research.